

Ejection-collision orbits in the RTBP

Mercè Ollé^a, Òscar Rodríguez^a, Jaume Soler^b

^a*Dept. Matemàtiques. Universitat Politècnica de Catalunya, Av Diagonal 647, 08028 Barcelona, Spain.*

^b*Dept. d'Enginyeria Civil i Ambiental. Universitat Politècnica de Catalunya, Av Diagonal 647, 08028 Barcelona, Spain.*

Abstract

In this paper we analyse the ejection-collision (EC) orbits of the planar restricted three body problem. As it is well known, for any value of the mass parameter $\mu \in (0, 1/2]$ and sufficiently restricted Hill regions, there are exactly four EC orbits. We check their existence and extend numerically these four orbits for $\mu \in (0, 0.5]$ and for less restrictive values of the Jacobi constant. We introduce the concept of n -ejection-collision orbits and we explore them numerically for $\mu \in (0, 0.5]$ and values of the Jacobi constant such that the Hill region containing the largest primary is bounded and does not contain the smaller one. We study the cases $1 \leq n \leq 10$ and we analyse the continuation of families of such n -EC orbits, varying the energy, as well as the bifurcations that appear.

Keywords: regularization, ejection-collision orbits, invariant manifolds, bifurcations.

2010 MSC: 70F07, 70F15

1. Introduction

We consider the restricted three-body problem (RTBP), which consists of the description of the motion of an infinitesimal body P under the attraction of two bodies called primaries, P_1 and P_2 of masses $m_1 = 1 - \mu$ and $m_2 = \mu$,
5 for $\mu \in (0, 0.5]$, which describe circular orbits around their common center of

Email addresses: Merce.Olle@upc.edu (Mercè Ollé), orodriguezdelrio@gmail.com (Òscar Rodríguez), jaume.soler.villanueva@upc.edu (Jaume Soler)

mass located at the origin. In particular, a solution of the RTBP has a collision (ejection) with the big primary P_1 at the instant t_0 if the distance between the particle and P_1 tends to zero when $t \rightarrow t_0^-$ ($t \rightarrow t_0^+$). An orbit defined on the interval (t_0, t_1) is called an ejection-collision orbit if it has an ejection when $t \rightarrow t_0^+$ and a collision when $t \rightarrow t_1^-$. This paper is devoted to the study of ejection-collision (EC) orbits.

Regarding analytical studies of EC orbits in the *planar* RTBP, Llibre [7] proved the existence of at least two EC orbits for $\mu > 0$ small enough and the energy H small enough (or equivalently the Jacobi constant C big enough). In Lacomba and Llibre [6] the authors used the existence of such transversal EC orbits to prove that both the Hill problem and the RTBP have no C^1 -extensible regular integrals. Chenciner and Llibre [3] proved the existence of four EC orbits for any value of $\mu \in (0, 1/2]$ and H small enough. Concerning the *spatial* RTBP Llibre and Martinez Alfaro [8] extended the existence of EC orbits for small enough values of the mass parameter. Finally in [9] and [12], the authors considered the *planar elliptic* RTBP and proved the existence of EC orbits for both the mass parameter and the eccentricity small enough. We remark that such results are obtained mainly applying blow up techniques, regularization of variables and perturbation approach.

Concerning numerical results, we mention Henon's paper about the computation of EC orbits obtained along the continuation of some families of symmetric periodic –non-collision– orbits in the Copenhagen problem (that is $\mu = 0.5$, see [4]) and also for Hill's problem (see [5]). Finally, the evolution of 16 particular collision periodic orbits obtained from the $\mu = 0.5$ case was numerically studied for various values of the mass ratio μ in [2].

In this paper we focus on what we call n -ejection-collision orbits, defined as EC orbits such that eject from the big primary P_1 , reach n times a relative maximum in the distance with respect to P_1 and finally collide with it. The approach is numerical and our goals are twofold: (i) On the one hand, we concentrate on 1-EC orbits. (i.1) We verify the existence of four 1-EC orbits for any value of $\mu > 0$ and very small values of H (known analytical results), (i.2)

we extend these results for any value of the mass parameter and less restrictive values of the energy obtaining families of 1-EC orbits when varying the energy for a fixed μ and (i.3) we analyse some bifurcations which appear. (ii) On the other hand, we make a similar study for n -EC orbits, with $n > 1$. As far as we know, there are no published results concerning parts (i.2), (i.3) and (ii).

The paper is divided as follows: Section 2 is devoted to a short description of the RTBP and some notation is introduced. In order to deal with the singularity arising from the zero distance between P and P_1 , we recall McGehee's ideas to regularize the equations of motion which become regular when P is at P_1 .

In Section 3 we describe the collision manifold, for any value of the mass parameter and we regard EC orbits as heteroclinic connections between different equilibrium points living on the collision manifold.

In Section 4 we focus on the n -EC orbits. We explain the numerical methodology used and describe the results for $1 \leq n \leq 5$. Finally we draw some conclusions.

2. The RTBP

The circular, restricted three-body problem (RTBP) describes the motion of a particle of infinitesimal mass, moving under the gravitational influence of two massive bodies, called primaries, that describe circular orbits around their common center of mass. We will consider the planar RTBP, in which the motion of the particle is contained in the plane of motion of the primaries. Taking a coordinate system that rotates with the primaries, with origin located at their center of mass, and suitable units, we can assume that the primaries have masses $1 - \mu$ and μ , $\mu \in (0, 1/2]$, their positions are fixed at $(-\mu, 0)$ and $(1 - \mu, 0)$, respectively, and the period of their motion is 2π . With these assumptions, the equations of motion for the particle in this rotating (also called synodical system) are given by

$$\begin{aligned} \ddot{x} - 2\dot{y} &= D_x\Omega(x, y) \\ \ddot{y} + 2\dot{x} &= D_y\Omega(x, y), \end{aligned} \tag{1}$$

where

$$\Omega(x, y) = \frac{1}{2}(x^2 + y^2) + \frac{1 - \mu}{\sqrt{(x + \mu)^2 + y^2}} + \frac{\mu}{\sqrt{(x + \mu - 1)^2 + y^2}} + \frac{1}{2}\mu(1 - \mu). \quad (2)$$

and $\dot{} = d/dt$.

It is well known that this system of ODE has the following properties (see [14] for details) which will be used along the paper:

1. It has a first integral, the so-called Jacobi integral, defined by

$$C = 2\Omega(x, y) - \dot{x}^2 - \dot{y}^2. \quad (3)$$

2. The equations of motion satisfy the symmetry

$$(t, x, y, \dot{x}, \dot{y}) \longrightarrow (-t, x, -y, -\dot{x}, \dot{y}). \quad (4)$$

This implies that given a solution for the particle, there exists another one which is symmetric with respect to the x axis (in the configuration projection (x, y)).

3. There exist 5 equilibrium points (with $(\dot{x}, \dot{y}) = (0, 0)$): the collinear ones, L_i , $i = 1, 2, 3$ on the x axis, and the triangular ones L_i , $i = 4, 5$ located at the vertices of an equilateral triangle with the primaries. We will assume that $x_{L_2} \geq 1 - \mu \geq x_{L_1} \geq -\mu \geq x_{L_3}$, that is, L_1 is between the primaries, L_2 is on the right hand side of the small one and L_3 on the left hand side of the big one. We will denote by $C_{L_i}(\mu)$ the value of the Jacobi constant at L_i for a given μ .

4. The equations of motion can be written as a Hamiltonian system in position (x, y) and momenta (p_x, p_y) variables, with $p_x = \dot{x} - y$ and $p_y = \dot{y} + x$, defined by the Hamiltonian function

$$H(x, y, p_x, p_y) = \frac{1}{2}(p_x^2 + p_y^2) + yp_x - xp_y - \frac{1 - \mu}{r_1} - \frac{\mu}{r_2} - \frac{1}{2}\mu(1 - \mu)$$

with $r_1 = \sqrt{(x + \mu)^2 + y^2}$ and $r_2 = \sqrt{(x + \mu - 1)^2 + y^2}$, and the relation between C and H is given by

$$H = -\frac{C}{2}. \quad (5)$$

We denote by $H_{L_i}(\mu)$, the associated value of the Hamiltonian at L_i for a given μ .

5. Fixed a value of the Jacobi constant C (or the Hamiltonian H), the motion is allowed to take place in the Hill's region defined by

$$\mathcal{R}(C) = \{(x, y) \in \mathbb{R}^2 \mid 2\Omega(x, y) \geq C\}.$$

In this paper we will restrict the range of values of C to $C \geq C_{L_2}(\mu)$ ($H \leq H_{L_2}(\mu)$, see in Figure 1 the corresponding Hill's regions). Actually, along the paper, we will use specific values of H , that can be translated to values of C through relation (5).

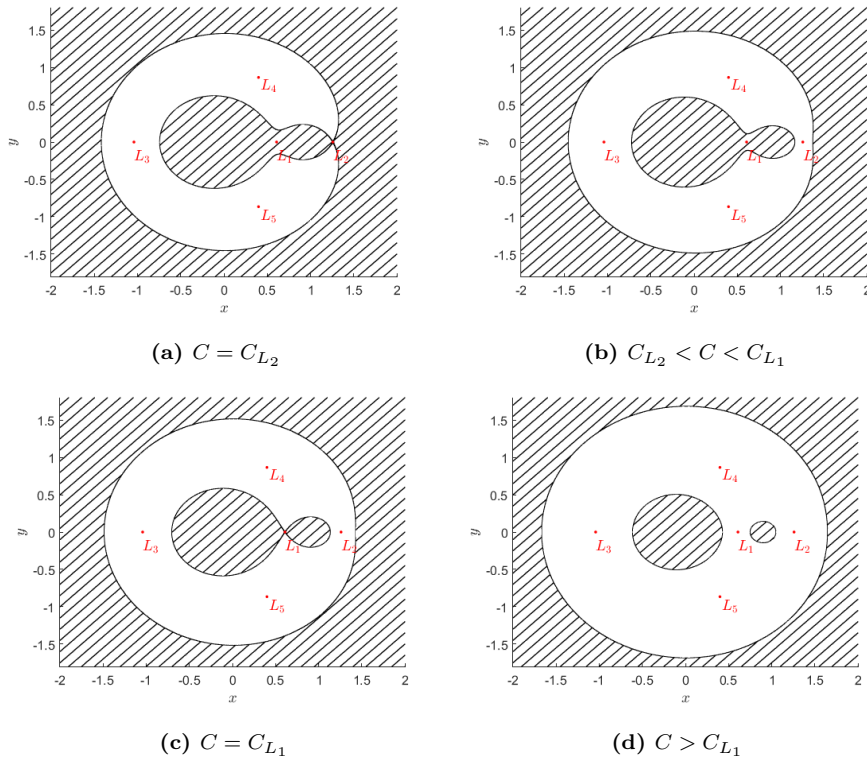


Figure 1: Hill's region according to the Jacobi constant C .

70 6. Regularization of the big primary. Since our goal is to study the ejection-collision orbits of the big primary, a first step is to deal with the singularity appearing in the equations when $r_1 = 0$.

To do so, we make a translation so that the primary of mass $1 - \mu$ is located

at the origin of coordinates and that of mass μ at $(1,0)$, that is, we consider $q_1 = x + \mu$, $q_2 = y$, $p_1 = p_x$, $p_2 = p_y$. In this reference system the Hamiltonian becomes (using the same notation H)

$$H(q_1, q_2, p_1, p_2) = \frac{1}{2}(p_1^2 + p_2^2) + p_1 q_2 - p_2 q_1 - \frac{1-\mu}{r_1} + \mu p_2 - \frac{\mu}{r_2} - \frac{1}{2}\mu(1-\mu), \quad (6)$$

with $r_1 = \sqrt{q_1^2 + q_2^2}$ and $r_2 = \sqrt{(q_1 - 1)^2 + q_2^2}$.

Now we introduce the canonical change of polar coordinates

$$\begin{aligned} q_1 &= r \cos \theta & p_1 &= p_r \cos \theta - \frac{p_\theta}{r} \sin \theta \\ q_2 &= r \sin \theta & p_2 &= p_r \sin \theta + \frac{p_\theta}{r} \cos \theta \end{aligned}$$

75 and the Hamiltonian (6) reads

$$\begin{aligned} H(r, \theta, p_r, p_\theta) &= & (7) \\ \frac{1}{2} \left(p_r^2 + \frac{p_\theta^2}{r^2} \right) - p_\theta - \frac{1-\mu}{r} + \mu \left(p_r \sin \theta + \frac{p_\theta}{r} \cos \theta \right) - \frac{\mu}{\sqrt{1+r^2-2r \cos \theta}} - \frac{1}{2}\mu(1-\mu) & (8) \end{aligned}$$

The associated Hamiltonian system of ODE is

$$\begin{aligned} \dot{r} &= p_r + \mu \sin \theta \\ \dot{\theta} &= \frac{p_\theta}{r^2} - 1 + \frac{\mu}{r} \cos \theta \\ \dot{p}_r &= \frac{p_\theta^2}{r^3} - \frac{1-\mu}{r^2} - \mu \frac{r - \cos \theta}{(1+r^2-2r \cos \theta)^{3/2}} + \mu \frac{p_\theta \cos \theta}{r^2} \\ \dot{p}_\theta &= \mu \left[-\frac{r \sin \theta}{(1+r^2-2r \cos \theta)^{3/2}} - p_r \cos \theta + \frac{p_\theta}{r} \sin \theta \right]. \end{aligned} \quad (9)$$

Applying McGehee's ideas (see [10] and [11]), we introduce the new variables

$$v = \dot{r} r^{1/2} \quad u = r^{3/2} \dot{\theta} \quad (10)$$

and a change of time $dt/d\tau = r^{3/2}$, such that the system of ODE becomes

$$\begin{aligned} r' &= vr \\ \theta' &= u \\ v' &= \frac{1}{2}v^2 + u^2 + 2ur^{3/2} + r^3 - (1-\mu) \\ &\quad - \mu r^2 \cos \theta - \mu r^2 \frac{r - \cos \theta}{(1+r^2-2r \cos \theta)^{3/2}} \\ u' &= -\frac{1}{2}uv - 2vr^{3/2} + \mu r^2 \sin \theta \left(1 - \frac{1}{(1+r^2-2r \cos \theta)^{3/2}} \right), \end{aligned} \quad (11)$$

where $' = d/d\tau$. We remark that the singularity $r = 0$ has been removed and this system has just one singularity –the collision with the small primary $r = 1$, $\theta = 0$. If we consider the hamiltonian (7) in these variables, which is a first integral, the relation $H = \mathfrak{H}$ becomes

$$0 = -r\mathfrak{H} + \frac{1}{2}(v^2 + u^2) - \frac{1}{2}r^3 - (1 - \mu) + \mu r^2 \cos \theta - \mu \frac{r}{\sqrt{1 + r^2 - 2r \cos \theta}} - \frac{1}{2}\mu r. \quad (12)$$

80 3. The collision manifold. Ejection/collision orbits.

System (11) has an invariant manifold Λ defined by $r = 0$, called the collision manifold. From (12) we conclude that Λ is a torus (see Figure 2),

$$\Lambda = \{u^2 + v^2 = 2(1 - \mu), \quad \theta \in [0, 2\pi]\} \quad (13)$$

and the dynamics on this torus is given by

$$\begin{aligned} \theta' &= u \\ v' &= \frac{1}{2}v^2 + u^2 - (1 - \mu) \\ u' &= -\frac{1}{2}uv. \end{aligned} \quad (14)$$

We want to point out that this torus is on the boundary of each energy level of the constant Hamiltonian (12).

For our purposes we remark that on Λ there exist two circles of equilibrium points defined by $S^+ = \{r = 0, \theta, v = v_0, u = 0, \theta \in [0, 2\pi]\}$ and $S^- = \{r =$
85 $0, \theta, v = -v_0, u = 0, \theta \in [0, 2\pi]\}$ with $v_0 = +\sqrt{2(1 - \mu)}$. We also observe that the tangent vector to both circles of equilibria is given by $(0, 1, 0, 0)$.

Let us define the matrices M^\pm as the linearization of system (11) at the corresponding equilibrium points S^\pm ; they are given by

$$M^\pm = \begin{pmatrix} \pm v_0 & 0 & 0 & 0 \\ 0 & 0 & 0 & 1 \\ 0 & 0 & v_0 & 0 \\ 0 & 0 & 0 & \mp v_0/2 \end{pmatrix},$$

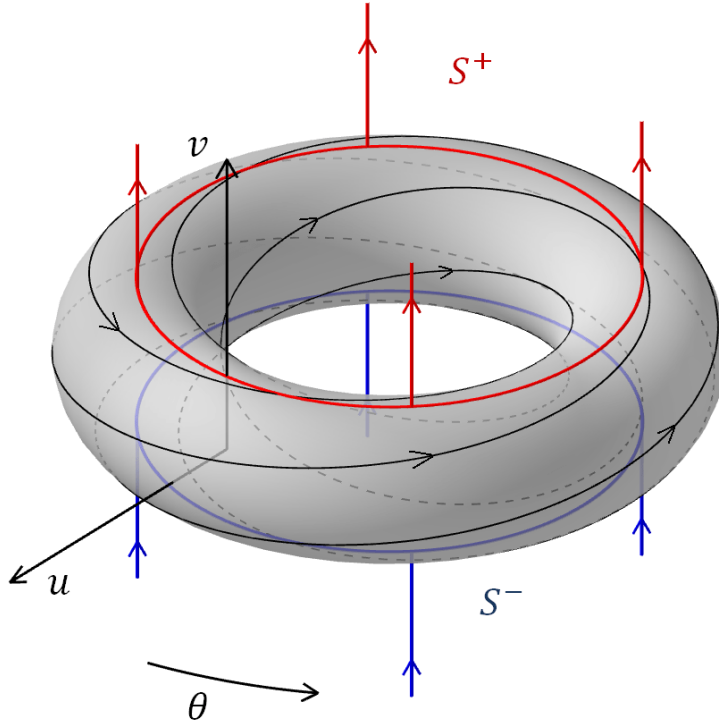


Figure 2: Collision manifold

The matrix M^+ has eigenvalues:

$$\lambda_1 = -v_0/2, \lambda_2 = \lambda_3 = v_0, \lambda_4 = 0$$

and corresponding eigenvectors:

$$\mathbf{v}_1 = (0, -2/v_0, 0, 1), \mathbf{v}_2 = (0, 0, 1, 0), \mathbf{v}_3 = (1, 0, 0, 0), \mathbf{v}_4 = (0, 1, 0, 0).$$

So for each equilibrium point $P \in S^+$ we have a 2-d unstable manifold
 90 $W^u(P)$ and a 1-d stable one $W^s(P)$. Similarly, for each equilibrium point
 $Q \in S^-$, we have a 2-d stable manifold $W^s(Q)$ and a 1-d unstable one $W^u(Q)$.

At this point we distinguish between 3 types of orbits: (i) ejection, (ii)
 collision and (iii) ejection-collision orbits.

(i) The set of ejection orbits –those which are ejected from collision with
 95 the big primary– is the set of orbits on the unstable manifold $W^u(P)$, for any

$P = (0, \theta, v_0, 0) \in S^+$. So each ejection orbit may be regarded as an orbit such that $r > 0$ for all finite time τ and asymptotically tends to an equilibrium point $P \in S^+$ as $\tau \rightarrow -\infty$.

(ii) The set of collision orbits –those which arrive at collision with the big primary– is the set of orbits on the stable manifold $W^s(Q)$, for any $Q = (0, \theta, -v_0, 0) \in S^-$. So each collision orbit may be regarded as an orbit such that $r > 0$ for all finite time τ and asymptotically tends to an equilibrium point $Q \in S^-$ as $\tau \rightarrow +\infty$.

(iii) The set of ejection-collision orbits –those which eject from/arrive at collision with the big primary– is the set of orbits obtained from the intersection $W^u(S^+) \cap W^s(S^-)$. So they may be regarded as heteroclinic orbits between $P \in S^+$ and $Q \in S^-$.

3.1. Particular case $\mu = 0$.

In order to have a first insight of such type of orbits, let us consider the particular case $\mu = 0$.

The manifold of ejection/collision orbits at the energy level $H = \mathfrak{H}$ is obtained from the condition $u = -r^{3/2}$ (the angular momentum is equal to 0), so

$$r\mathfrak{H} = \frac{1}{2}v^2 - 1. \quad (15)$$

We plot in Figure 3 the associated level curves and in Figure 4 we visualize the corresponding manifolds in variables (r, θ, v) . In particular, for $H = \mathfrak{H} < 0$ we obtain the coinciding manifolds of ejection-collision orbits. If $H = \mathfrak{H}$ is either equal to 0 or positive, we obtain the manifolds consisting of the ejection-parabolic escape orbits (and parabolic escape-collision ones) and the ejection-hyperbolic escape orbits (and hyperbolic escape-collision ones) respectively, in the sense that they arrive at (depart from) infinity with zero or positive velocity.

We are particularly interested in this paper in ejection-collision orbits. We have just shown that for $\mu = 0$ the ejection manifold and the collision one coincide for $H < 0$. Thus any orbit ejecting from the primary ends colliding with it.

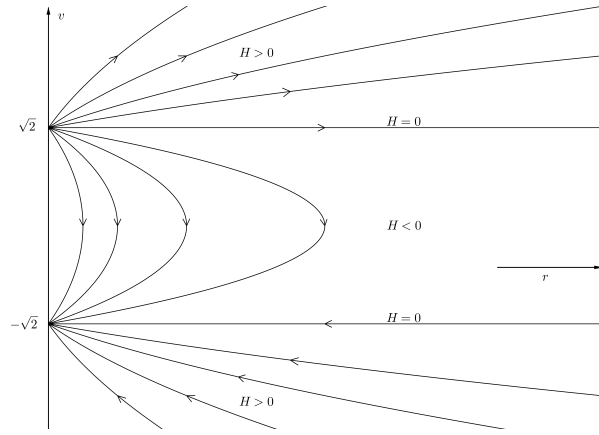


Figure 3: $\mu = 0$. Level curves of $rH = \frac{1}{2}v^2 - 1$

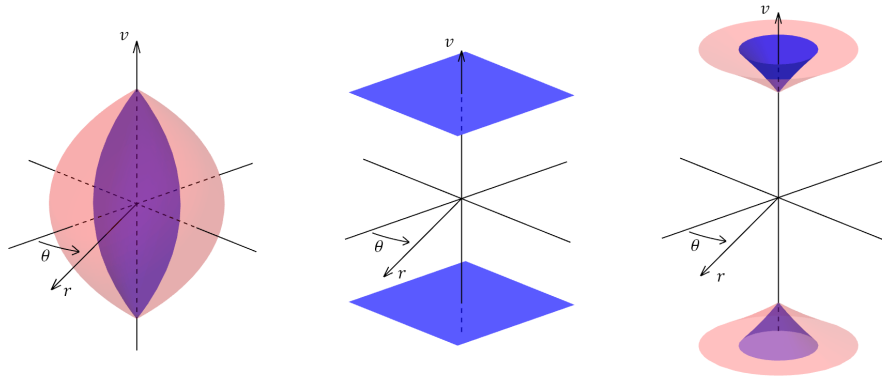


Figure 4: $\mu = 0$. Ejection-collision manifold for $H < 0$ (left). Ejection and collision manifolds for $H = 0$ (middle) and $H > 0$ (right).

Now we want to study the general case $\mu \neq 0$ and $H < 0$. When μ is different from zero, the influence of the small primary somewhat deforms the ejection and collision manifolds and these manifolds do not coincide any more.

125 The dynamics is much richer and intricate in this case.

The subject of the next Sections is to study, from a numerical point of view, this dynamics.

4. n -Ejection-collision orbits

We are now focused on what we call n -ejection-collision orbits, simply noted
 130 by n -EC orbits, that is orbits that eject from the big primary and reach n times
 a relative maximum in the distance r before colliding with the big primary. See
 Figure 5.

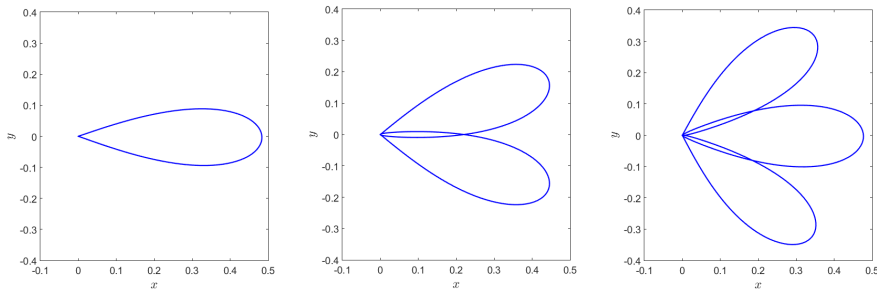


Figure 5: Examples of n -ejection-collision orbits for $n = 1, 2, 3$ (from left to right). For
 $n = 2$ ($n = 3$), there is 1 (2) close passages to collision between ejection and collision.

For the particular case $n = 1$, it is proved analytically in [3] that, for $H =$
 $\mathfrak{H} < 0$ small enough and any value of $\mu \in (0, 1/2]$, there exist exactly four 1-
 135 ejection-collision orbits. We remark, however, that the Hill's regions considered
 in that paper are very restrictive.

In this section, we will generalise the previous results in two directions. On
 the one hand, concerning 1-EC orbits, we will show that these four 1-EC orbits
 exist for any value of the mass parameter $\mu \in (0, 0.5]$ and less restrictive Hill's
 140 regions, and we analyse some bifurcations as well as the existence of some new
 families. On the other hand, the existence of n -ejection-collision orbits ($n \geq 2$)
 for any value of the mass parameter and $H \leq H_{L_1}(\mu)$ is also analysed, families
 of n -EC orbits are computed and the appearing bifurcations are discussed.

But first let us shortly describe the numerical methodology used to deal with
 145 EC orbits.

4.1. Numerical methodology

A first goal is the computation of the ejection (collision) orbits, that is,
 we need to compute the unstable (stable) manifold of any equilibrium point

belonging to S^+ (S^-), denoted by $W^u(S^+)$ ($W^s(S^-)$). To do so, fixed a value of $H = \mathfrak{H}$, in order to consider initial conditions for an ejection orbit, we make two comments: on the one hand, for each equilibrium point $P \in S^+$, the 2-d $W^u(P)$ is tangent to the plane passing through P generated by the eigenvectors \mathbf{v}_2 and \mathbf{v}_3 (see Section 3), i.e. vectors like $\mathbf{v} = (\beta, 0, \gamma, 0)$, with $\beta, \gamma \in \mathbb{R}$. On the other hand, we recall that the energy level set $H = \mathfrak{H}$ is defined implicitly by (12), and the normal vector to this energy level set at point $P = (0, \theta_0, v_0, 0)$ is $\mathbf{n} = (-\mathfrak{H} - \frac{3}{2}\mu, 0, v_0, 0)$. So the vectors \mathbf{v} (generating the tangent plane $W^u(P)$) must be perpendicular to \mathbf{n} , i.e. they must satisfy

$$\beta(-\mathfrak{H} - \frac{3}{2}\mu) + \gamma v_0 = 0.$$

It is clear that such vectors are contained in the plane (r, v) and are tangent to the ejection orbit at the point $(0, \theta, v_0, 0)$. So we will take the initial condition of an ejection orbit associated with the point $P = (0, \theta_0, v_0, 0)$ as

$$(0, \theta_0, v_0, 0) + s \frac{\mathbf{w}}{\|\mathbf{w}\|} \quad (16)$$

with $\mathbf{w} = (1, 0, (\mathfrak{H} + \frac{3}{2}\mu)/v_0, 0)$ and $s > 0$ a small quantity (typically 10^{-6}). Varying $\theta_0 \in [0, 2\pi]$, we generate a set of initial conditions belonging to the (tangent plane to the) unstable manifold $W^u(S^+)$ for $H = \mathfrak{H}$ fixed. For each
150 initial condition we integrate the system (11) forward in time.

We have done several tests taking different values of s (ranging from 10^{-7} to 10^{-5}) giving rise to the same results.

We proceed similarly in order to obtain a set of initial conditions of the collision orbits belonging to the stable manifold $W^s(S^-)$ for $H = \mathfrak{H}$ fixed. For
155 each initial condition, we integrate system (11) backward in time.

Once we know how to obtain ejection and collision orbits, a second goal is to focus our attention on showing the existence of n -EC orbits. For this purpose, we distinguish between two different strategies. Both methods require the computation of the intersection of the flow of system (11) with the Poincaré
160 section $\Sigma : g(\mathbf{x}) = g(r, \theta, v, u) = v = 0$. To obtain numerically such Poincaré section, we remark that given an initial condition \mathbf{x} and the associated solu-

tion $\phi(t, \mathbf{x})$, we apply a Newton's method to obtain a suitable $\tilde{\tau}(\mathbf{x})$ such that $g(\phi(\tilde{\tau}(\mathbf{x}), \mathbf{x})) = 0$.

The two strategies to compute n -EC orbits are the following

165 *Method 1: Intersection of the manifolds $W^u(S^+)$, $W^s(S^-)$ with Σ .*

For a fixed H , let us denote Σ_n , the n -th crossing with Σ and define $D_n^+ = W^u(S^+) \cap \Sigma_n$, and $D_n^- = W^s(S^-) \cap \Sigma_n$. In this first strategy, we look for intersection points belonging to $D_n^+ \cap D_n^-$. Any such point corresponds to an n -EC orbit.

170 For example, we take the particular values of $\mu = 0.5$ and $H = H_{L_1}(0.5) = -2.125$. In Figure 6 left, $W^u(S^+)$ and $W^s(S^-)$ are shown up to Σ_1 in variables (x, y, v) , and the right Figure displays the resulting curves D_1^+ and D_1^- in (x, y) variables. We can see that both curves intersect at four points which correspond to four 1-EC orbits (for these values of μ and H).

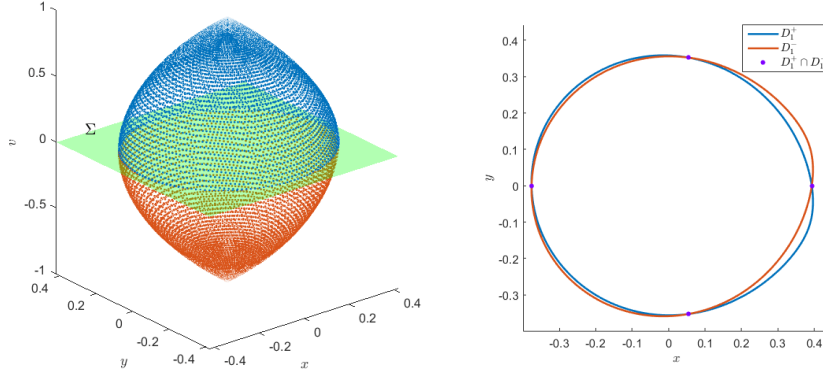


Figure 6: *Left.* $W^u(S^+)$ (ejection orbits in blue) and $W^s(S^-)$ (collision orbits in red) up to Σ_1 for $\mu = 0.5$ and $H_{L_1}(0.5)$. *Right.* The associated curves D_1^+ and D_1^- .

175 At this point several remarks must be made:

1. Due the symmetry (4), we only need to compute D_n^+ , and apply the symmetry to obtain D_n^- and then plot the intersection $D_n^+ \cap D_n^-$.

2. The curve D_n^+ (D_n^-) obtained numerically is actually a discrete set of points (obtained from the discrete set of initial conditions and integrating each orbit up to Σ_n). This discrete curve is enough to show the existence of n -EC orbits

180

with a simple plot (taking a large enough set of initial conditions, plotting the intersection curves D_n^+ , D_n^- and looking at the number of intersection points in $D_n^+ \cap D_n^-$).

However, in order to describe a particular EC orbit, we need to know its
 185 precise initial conditions, that is, the precise θ_0 once s is fixed, from (16). So we need to get the *continuous* curve D_n^+ (D_n^-) parameterized by the angle $\theta_0 \in [0, 2\pi]$. To do so, we just consider linear interpolation. Therefore any particular desired n -EC orbit can be obtained from the intersection of both continuous curves, $D_n^+ \cap D_n^-$.

3. The previous approach will be useful and easy for $n = 1$, since the curves
 190 D_n^+ and D_n^- look as nice near circles (for the ranges of H considered). However for $n \geq 2$, such curves are more intricate. For $n = 2$ the curves D_2^+ , D_2^- are only piecewise defined. Each curve D_1^+ (or D_1^-) gives rise to four pieces –which compose D_2^+ (D_2^-)– due to the existence of four 1-EC orbits for $H \leq H_{L_1}(\mu)$
 195 (see for example Figure 7 where curve D_2^+ is shown) and it is not straightforward to apply method (i) to look for the intersection $D_2^+ \cap D_2^-$. Even a more intricate situation takes place for $n > 2$.

So, we will apply the following appropriate alternative method.

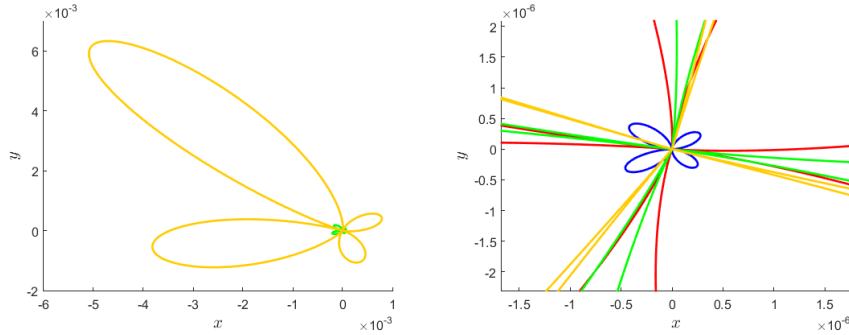


Figure 7: D_2^+ in variables (x, y) for $\mu = 0.5$ and values of H -5.25 in blue, -3.25 in red, -2.75 in green for $H_{L_1}(\mu)$ in yellow. On the right: blow up.

Method 2: Singularity in time

200 In this method and for fixed H , we take the set of initial conditions of ejection

orbits, parameterized by $\theta_0 \in [0, 2\pi]$, we consider the Σ_{2n} intersection of the ejection orbits i.e. $W^u(S^+) \cap \Sigma_{2n}$ (similarly we might consider $W^s(S^-) \cap \Sigma_{2n}$) and we look for vertical asymptotes in time T_{2n} in the curve (θ_0, T_{2n}) , $\theta_0 \in [0, 2\pi]$ (T_j being the necessary time to reach Σ at the j -th crossing). Moreover we
205 compare this curve with the one (θ_0, T_{2n-2}) (or we might also consider the curve (θ_0, T_{2n-1})) in order to identify only the *new* vertical asymptotes in time T_{2n} that do not appear in the curve (θ_0, T_{2n-2}) , which will correspond to the n -EC orbits specifically.

More precisely, for $n = 1$ and fixed H , we compute the curve (θ_0, T_2) , for
210 $\theta_0 \in [0, 2\pi]$. Since 1-EC orbits are heteroclinic connections between a point $P = (0, \theta_0, v_0, 0) \in W^u(S^+)$ and a point $Q \in W^s(S^-)$ with just one path through maximum distance in r , the curve (θ_0, T_2) should have a vertical asymptote in T_2 for each θ_0 corresponding to a 1-EC orbit. We will say that each such θ_0 is a *singularity*.

For example, in order to identify the 1-EC orbits, we show in Figure 8 the
215 curve (θ_0, T_2) for $\mu = 0.5$ and $H = H_{L_1}(0.5)$. Each value of θ_0 such that T_2 becomes unbounded is an initial condition of a 1-EC orbit. We observe four asymptotes, i.e. four 1-EC orbits in accordance with method 1. We also observe that the curve (θ_0, T_2) is composed of four U-shaped curve branches
220 (each branch begins and ends at an asymptote).

A similar approach is applied to n -EC orbits taking into account the curve
 (θ_0, T_{2n}) . Of course in this curve we have *all* the singularities (vertical asymptotes in time) corresponding to EC orbits, so in order to detect the actual n -EC orbits, we will take into account only the singularities appearing in the
225 curve (θ_0, T_{2n}) and not in the curve (θ_0, T_{2n-2}) , to discard the j -EC orbits, for $j = 1, \dots, n - 1$.

The natural question arises: in order to compute a precise 1-EC orbit (or
 n -EC orbit in general), how do we compute the precise value of θ_0 (i.e. its initial condition, for s fixed), such that T_2 (T_{2n}) becomes unbounded? The key
230 stone is that along each U-shaped curve branch the value of u remains constant in sign and it changes sign consecutively as we change the U-shaped branch,

when increasing $\theta_0 \in [0, 2\pi]$. Precisely at the boundary of each branch u is equal to 0 (since an EC orbit is a heteroclinic orbit connecting two equilibrium points with $u = 0$). So in order to find a particular 1-EC orbit (n -EC orbit), we simply apply a bisection method on a suitable interval of θ_0 such that there is an asymptote in between, i.e. a zero on u at the second crossing with Σ (or at the $2n$ -th crossing in general).

Finally, we point out that we have used double precision throughout all the computations and a Runge-Kutta-Fehlberg 8(7) method in order to integrate numerically the system of ODE given by (11).

4.2. Results for 1-EC orbits

4.2.1. Existence of four 1-EC orbits.

We have considered a grid of values of μ in the interval $[0.01, 0.5]$ and for any given μ and fixed $H \leq H_{L_1}(\mu)$, we have applied method 1, i.e. we have taken a set of initial conditions (parametrized by $\theta_0 \in [0, 2\pi]$ according to (16)) of ejection orbits belonging to $W^u(S^+)$, we have computed $D_1^+ = W^u(S^+) \cap \Sigma_1$ (similarly D_1^-) and their intersection $D_1^+ \cap D_1^-$. Let us denote $(r_0, \theta_0, v_0, u_0)$ (with $u_0 = 0$) the initial condition of an ejection orbit, and $(r_i, \theta_i, v_i, u_i)$ the values of (r, θ, v, u) of this orbit at Σ_i (i -th intersection with Σ).

We have obtained qualitatively the same kind of results for any μ . The numerical simulations carried out confirm not only the analytical results for any μ and H small enough: existence of four 1-EC orbits, but also that this result also holds true for any $\mu \in (0, 0.5]$ and $H \leq H_{L_1}(\mu)$.

To show the numerical results obtained, we take, for example, $\mu = 0.5$ (for other values of μ see [13]). In Figure 9 we show the manifolds $W^u(S^+)$ and $W^s(S^-)$ (up to Σ_1) for $\mu = 0.5$ and different values of H (Figure 9 left). We also plot the corresponding curves D_1^+ and D_1^- and the projection of the 1-EC orbits in the (x, y) variables (Figure 9 right). We clearly see four 1-EC orbits for each value of H . Concerning the symmetries of these 1-EC orbits, and due to (4), we point out that two of them cross the x axis (i.e. $\theta_1 = 0, \pi$) when they intersect with Σ (so $\dot{x} = 0$) and the projection of each of these two orbits in the

(x, y) variables is symmetric with respect to the x ; the $((x, y))$ projection of the other two EC orbits are non-symmetric but one of them can be obtained from the other one applying the x axis symmetry. See Figure 9 right.

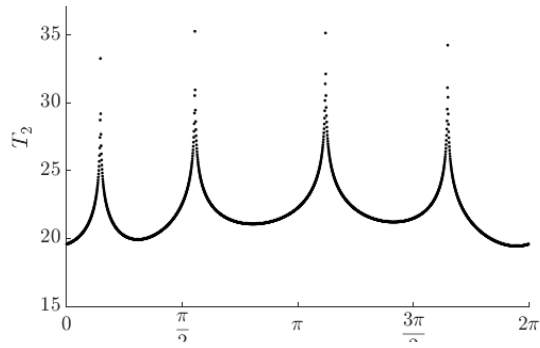


Figure 8: Curve (θ_0, T_2) for $\mu = 0.5$ and $H_{L_1}(0.5)$.

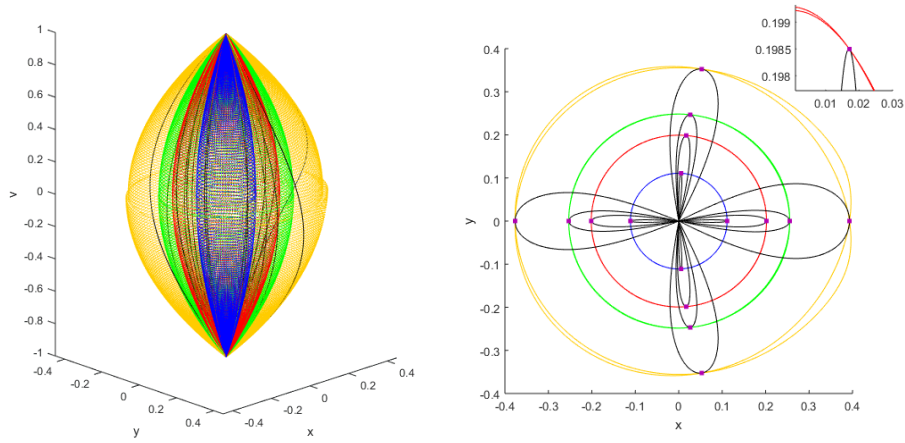


Figure 9: *Left.* $W^u(S^+)$ (ejection orbits) and $W^s(S^-)$ (collision orbits) up to Σ_1 for $\mu = 0.5$ and values of H -5.25 in blue, -3.25 in red, -2.75 in green and $H_{L_1}(\mu)$ in yellow. In black the 1-EC orbits for such values of H . *Right.* Associated D_1^+ and D_1^- . In purple the points of the EC orbits at Σ_1 and in black the projections of the EC orbits on the configuration plane (x, y) .

265

Now let us describe the results applying method 2.

In order to show the results obtained with this method, we only need to

compute T_i (the necessary time to reach Σ_i). In Figure 10 we plot the curves (θ_0, T_2) (left) and (θ_1, T_2) (right) for $\mu = 0.5$ and different values of H . In accordance with the previous method, from the left plot (using (θ_0, T_2)) we can conclude that for any μ and H considered, there are four 1-EC orbits. From the right one, (using (θ_1, T_2)), we have the additional information about the symmetry of the (x, y) projection of such EC orbits (applying (4)): there are always two 1-EC orbits symmetric with respect to the x axis ($\theta_1 = 0, \pi$) and two non symmetric orbits such that one can be obtained from the other one (if one of them has $\theta_1 = \sigma$ then the other one has $\theta_1 = 2\pi - \sigma$).

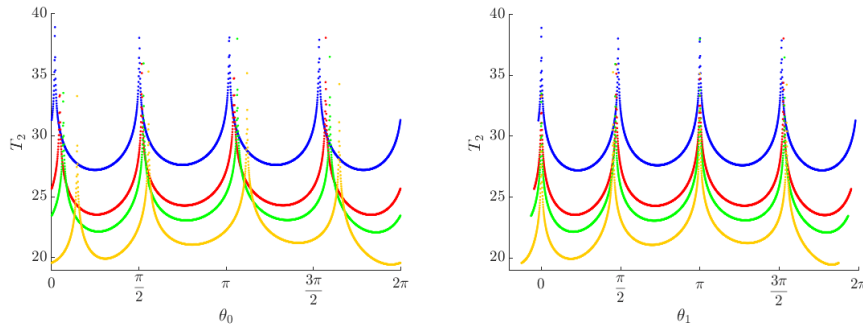


Figure 10: T_2 as a function of θ_0 (left) and θ_1 (top) and $\mu = 0.5$ and values of H -5.25 in blue, -3.25 in red, -2.75 in green and $H_{L_1}(0.5)$ in yellow.

4.2.2. Families of 1-EC orbits. Bifurcations

It is clear, from the Hill regions, that for $H < H_{L_1}(\mu)$ the ejection motion is restricted to a bounded permissible region around the big primary m_1 (see Figure 1). The goal of this Section is to give an insight, concerning EC orbits, of the richness of the dynamics that can take place as far as $H \geq H_{L_1}(\mu)$, due to not only the presence of both primaries, but also the chaotic involved dynamics because of the existence of unstable periodic orbits and their invariant manifolds (just take into account the Lyapunov periodic orbits for instance, see [1] and references therein). In particular, new bifurcating families of 1-EC orbits appear.

So applying method 2 we do a massive simulation in order to detect the four

families of 1-EC orbits, when varying $H \leq H_{L_2}(\mu)$ for any given $\mu \in (0, 0.5]$. We call such families α , β , γ and δ . The results are shown in Figure 11 for $\mu = 0.5$. We call *diagram* (θ_0, H, T_2) , the plot where we obtain T_2 as a function of the angle θ_0 and the energy H . For a fixed H , the four angles θ_0 for which T_2 is large, correspond to the four particular values of θ_0 for which there exist 1-EC orbits.

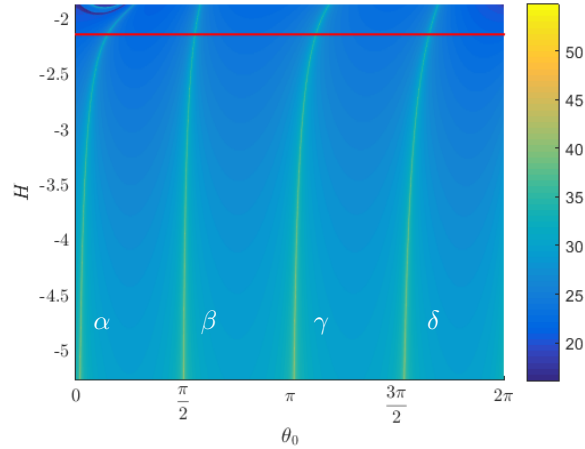


Figure 11: Diagram (θ_0, H, T_2) for $\mu = 0.5$ for values of $H \leq H_{L_2}(0.5)$. The red line corresponds to $H_{L_1}(0.5)$.

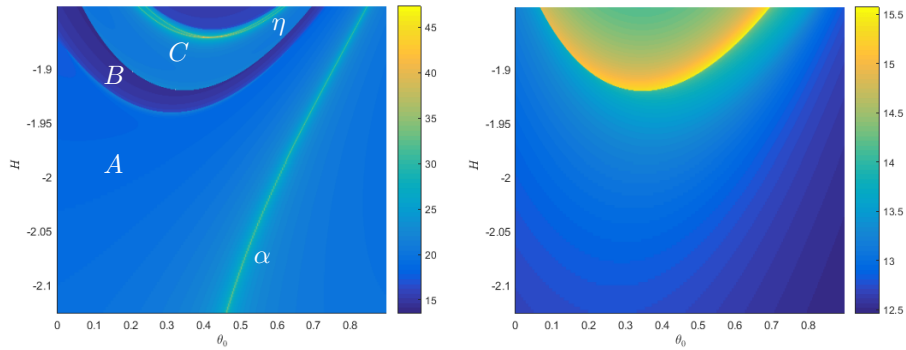


Figure 12: Zoom of diagram (θ_0, H, T_2) (*left*) and (θ_0, H, T_1) (*right*) for $\mu = 0.5$

We remark from this Figure, that for $H_{L_1}(\mu) < H$ there appear new bifurcated families (although difficult to be seen in the Figure). Let us describe this phenomenon for $\mu = 0.5$ and $-2.125 = H_{L_1}(0.5) < H < H_{L_2}(0.5) =$

-1.853398112043077.

In Figure 12 we plot a zoom in a neighbourhood of the α family. We observe apparently a new family which we call η . But before describing this bifurcation, we remark three different regions, labelled by A , B and C . First of all, we see
 300 that the ejection orbits that live in A and C have a similar value of T_2 , but a smaller one for the region B in between.

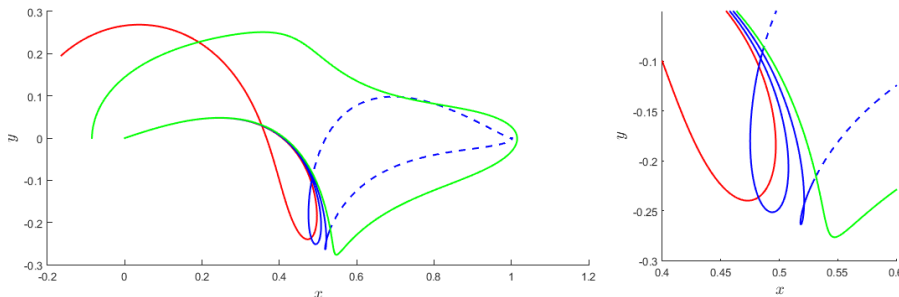


Figure 13: Different ejection orbits belonging to region A (red), B (blue) and C (green) for $\theta_0 = 0.4$ (left) and a zoom around the turning point of the same orbits (right). All of them have a continuous path for time up to T_2 and a discontinuous path only for those orbits in region B and along the range of time from T_2 up to T_3 .

The behaviour of the orbits in these regions is the following (see Figure 13): orbits in region A do not have enough energy to go to the small primary and they behave in a usual way, starting at ejection with the big primary, having
 305 a loop and returning close to it (see orbit red in the Figure). Those orbits in region B (in blue) do have enough energy to go close to the small primary, but not enough energy to go in a direct path, they describe a small loop before getting there. Just short after the loop they reach T_2 and that is the reason why T_2 is smaller in the region B (see the continuous small loop of the two orbits
 310 in blue in Figure 13). Finally those orbits in region C have enough energy to visit the small primary and return back (close) to the big one, along the time T_2 (see the long green orbit in the Figure).

Of course, this behaviour for the orbits is reflected in the diagram (θ_0, H, T_1) , see Figure 12 right, where the boundary between regions B and C is clearly

315 seen. Along the yellow region in the Figure 12 right we observe how T_1 is sensitively bigger since for this region, the loop does not exist, the orbits visit a neighbourhood of the small primary m_2 and they need a larger time to reach Σ . See also Figure 13.

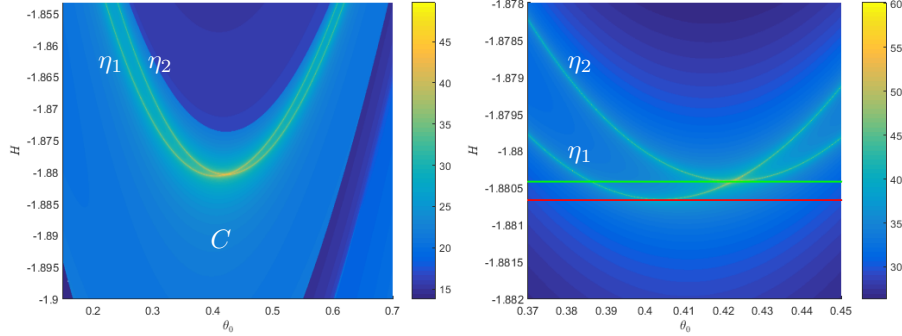


Figure 14: Zoom (of Figure 12) of the new bifurcated families. Red and green horizontal lines correspond to $H = H_{b_1}$ and $H = H_{b_2}$ respectively.

Let us focus now on the bifurcated family η (see Figure 12). These new
 320 EC orbits detected correspond to orbits that visit the region close to the small primary at his first intersection with Σ . If we zoom this region (see Figure 14) around η , we observe actually two different curves, that is two different bifurcated families, which we label η_1 and η_2 : when increasing H , the first family that appears is η_1 , at a particular minimum value $H = H_{b_1}$. As far as
 325 h increases, a new branching point appears at $H = H_{b_2}$, and we obtain a new family labelled η_2 . 1-EC orbits belonging to η_1 are symmetric with respect to the x axis. In Figure 15 left, we plot the EC orbit (in blue) for H_{b_1} where η_1 is born, and in red and in green the two corresponding 1-EC orbits of family η_1 for two increasing fixed values of H . 1-EC orbits belonging to η_2 are non symmetric.
 330 In Figure 15 right, we plot the EC orbit (in blue) for H_{b_2} that belongs to η_1 and where η_2 is born, and in red and in green the two corresponding 1-EC orbits of family η_2 for two increasing fixed values of H .

Therefore we can conclude that the existence of only four 1-EC orbits is no longer true for higher values of the energy H , since there appear new ones. We
 335 plot in Figure 16 eight 1-EC orbits for $\mu = 0.5$ and $H_{L_2}(0.5)$, together with the

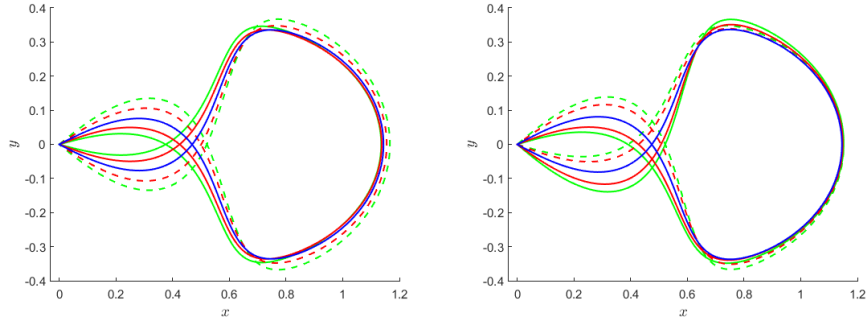


Figure 15: 1-EC bifurcated orbits belonging to η_1 (left, for $H = H_{b1}$ in blue, for a value $H > H_{b1}$ in green and in red) and η_2 (right, for $H = H_{b2}$ in blue, for a value $H > H_{b2}$ in green and in red).

Hill's region.

A final remark is that the bifurcation described for $\mu = 0.5$ also may take place for other small values of μ and less restrictive Hill's regions (higher values of H). Of course, as far as the Hill's regions allow non-bounded motions, a very rich dynamics starting at ejection with the big primary takes place. But this is a more intricate study which will be done in a next future.

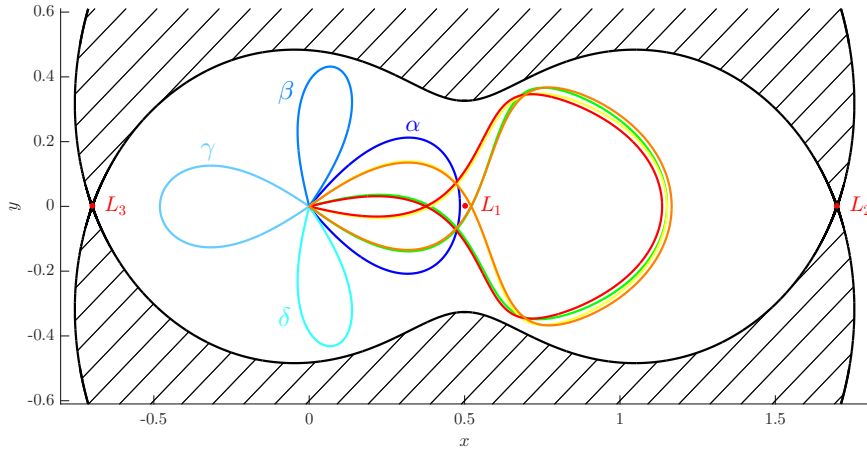


Figure 16: (x, y) projection of the eight 1-EC orbits that exist for $\mu = 0.5$ and $H_{L_2}(\mu)$. In blue the known ones and in other colours the new bifurcated orbits.

4.3. Results for n -EC orbits. Families and bifurcations.

Recall that an n -ejection-collision orbit is an orbit which ejects from the first primary and collides again after the distance to this primary has reached n times a relative maximum (see Figure 5). As stated in section 4.1 describing the numerical methodology, method 2 is more suitable to study n -EC orbits.

We have done massive simulations applying method 2 for any value of $\mu \in [0.01, 0.5]$ and for a fixed μ , we have considered energy levels below $H_{L_1}(\mu)$ (in order to avoid collision with the second primary; since we take long time integration of the equations, the influence of the second primary makes the dynamics more and more intricate for increasing values of n). The results are qualitatively similar for any value of μ .

The numerical results obtained show that for all $\mu \in (0, 0.5]$ and all n there exists an $\hat{H}(\mu, n)$ such that for $H \leq \hat{H}(\mu, n)$ there exist four n -ejection-collision orbits, which can be characterized in a way similar to the characterization of the 1-ejection-collision orbits:

- There are two of them which intersect the x -axis (i.e. $\theta_n = 0, \pi$) when they intersect the Poincaré section Σ_n . They are symmetric with respect to the x axis (taking the (x, y) projection). We will follow the previously used notation and call the corresponding families (when varying H) α_n and γ_n respectively.
- The other two (which do not intersect the x -axis when they cross the Poincaré section Σ_n) are non symmetric with respect to the x -axis (taking the (x, y) projection), but one can be obtained from the other one applying symmetry (4). Following again the notation previously introduced we will call the corresponding families β_n and δ_n , respectively.

We show examples of orbits belonging to families α_n , β_n , γ_n and δ_n , for $n = 2$ and $n = 3$ in Figure 17 for $\mu = 0.1$ and different values of H .

In order to show the families of n -EC orbits, for $n \geq 2$, when varying H , we will use the diagram (θ_0, H, T_{2n}) as we did for $n = 1$. However, we must take

into account, that the diagram (θ_0, H, T_{2n}) , contains the families of n -EC orbits and the families of 1-EC, ..., $(n - 1)$ -EC orbits as well. Therefore to detect the actual families of n -EC orbits, we must take into account the new singularities that do not appear in the diagrams (θ_0, H, T_{2j}) , for $j = 1, \dots, n - 1$. In Figure 18, we take $\mu = 0.1$ and we show the diagrams (θ_0, H, T_{2n}) , for $n = 1, \dots, 5$ and $H \leq H_{L_1}(0.1) = -1.843476614939948$. Thus, we observe that for each $n = 1, \dots, 5$, there exist four families of 2, ..., 5-EC orbits, taking as parameter the value of H up to a suitable one, $H \leq \hat{H}(\mu, n)$.

However, for high values of n and H , the statement about the existence of four families of n -EC orbits can no longer be true because of the influence of the other primary and a rich dynamics. We will focus on two particular phenomena: (i) the intersection of families and (ii) bifurcation of families.

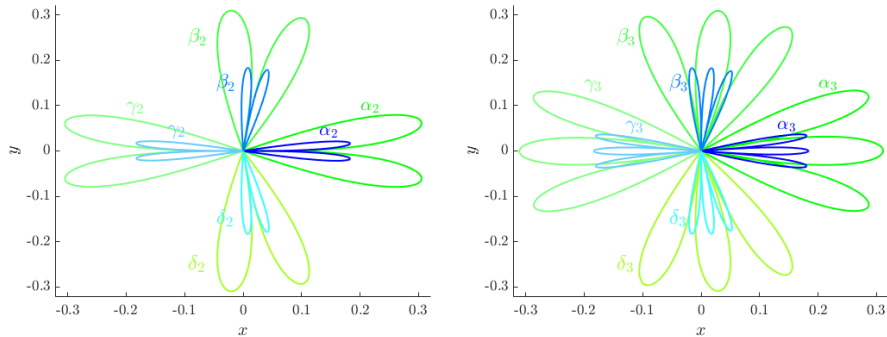


Figure 17: The four n -ejection-collision orbits for $\mu = 0.1$ and $n = 2$ (left) and $n = 3$ (right) for $H = -5.05$ (blue) and $H = -3.05$ (green)

Concerning (i), if we consider the new singularities obtained at the $2n$ -th intersection with Σ , i.e. the initial values θ_0 of the n -EC orbits (giving rise to the yellow curves in the (θ_0, h, T_{2n}) diagram), and these singularities intersect some of the previously obtained ones, i.e. singularities in the k -th intersection with Σ for $k < 2n$, then there are no n -EC orbits because, for those corresponding values of θ_0 , the orbit has already had a previous collision. This phenomenon can be seen with more detail in Figure 19, where the colour of the T_{10} variable has been rescaled in the amplification for easier viewing.

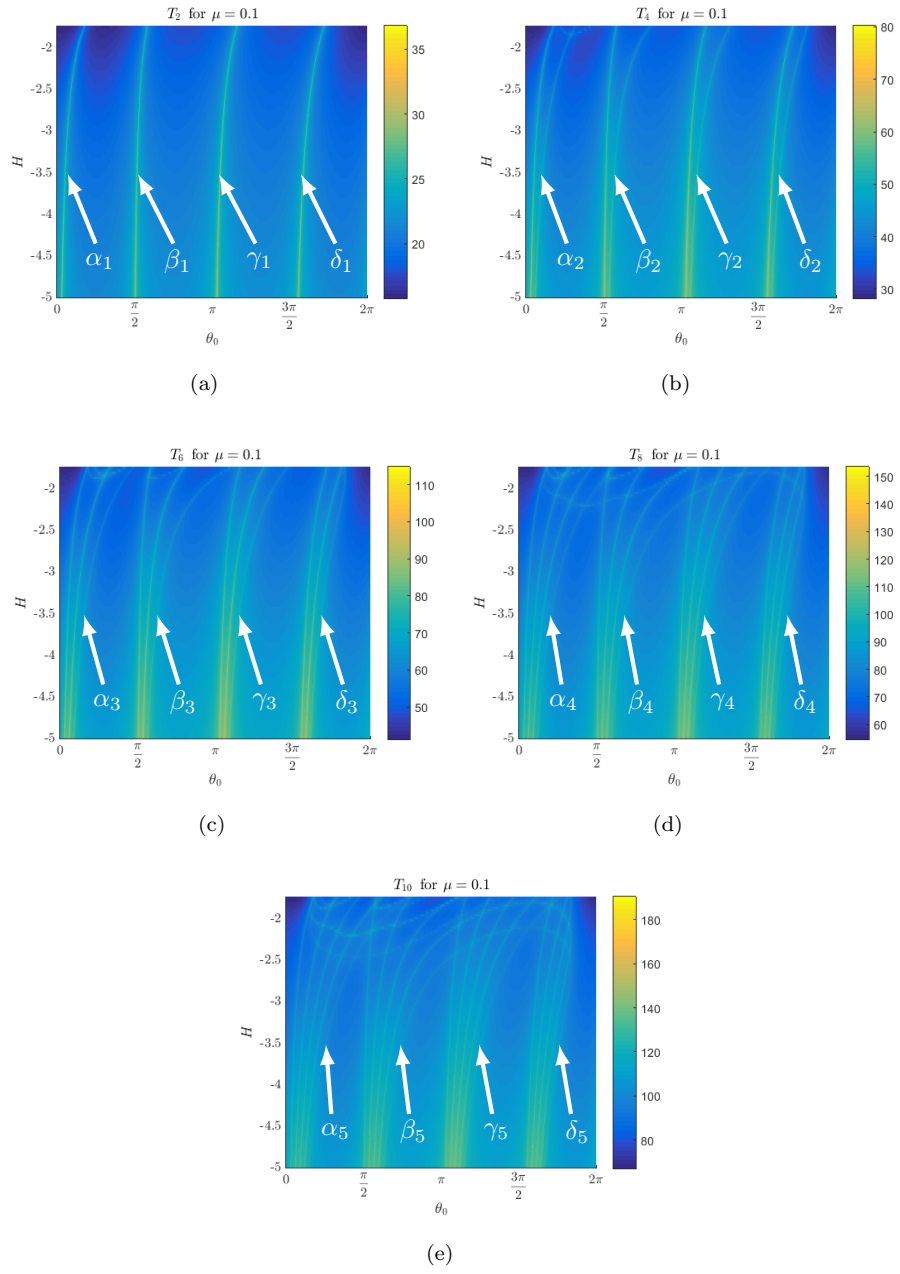


Figure 18: From left to right and top to bottom values of T_{2i} for $i = 1, \dots, 5$ as a function of θ_0 and H for $\mu = 0.1$

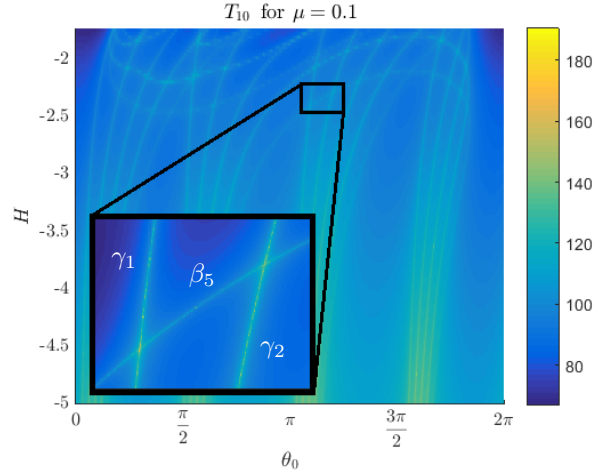


Figure 19: Zoom of the diagram (θ_0, H, T_{10}) , for $\mu = 0.1$ with the intersection of singularities.

Concerning (ii), we observe, when increasing H , the termination of families or collapse of two different families on to a singularity belonging to another different family. This is the situation shown in Figure 20 for $\mu = 0.1$, where the two families of non-symmetric EC orbits, β_4 and δ_4 collapse on to a symmetric EC belonging to family γ_4 . In other words, if we consider the families when decreasing the H parameter, we would say that the two families β_4 and δ_4 have bifurcated from the family γ_4 at the collapsing orbit.

Finally, there is another type of bifurcation when increasing the H parameter and it is related to the appearance of new bifurcating families from the main four families. This is the same type of bifurcation mentioned in the case of 1-EC families. For example, we show in Figure 21, the new bifurcating families α_4^1, α_4^2 of non-symmetric 4-EC orbits from family α_4 , for $\mu = 0.1$ (we show a zoomed diagram (θ_0, H, T_8) from the one in Figure 18, as well as the bifurcating orbit and two orbits of each family for different values of H).

5. Conclusions

We have studied the n -EC orbits for different values of n and energy H and we have obtained similar results for any value of the mass parameter. We have

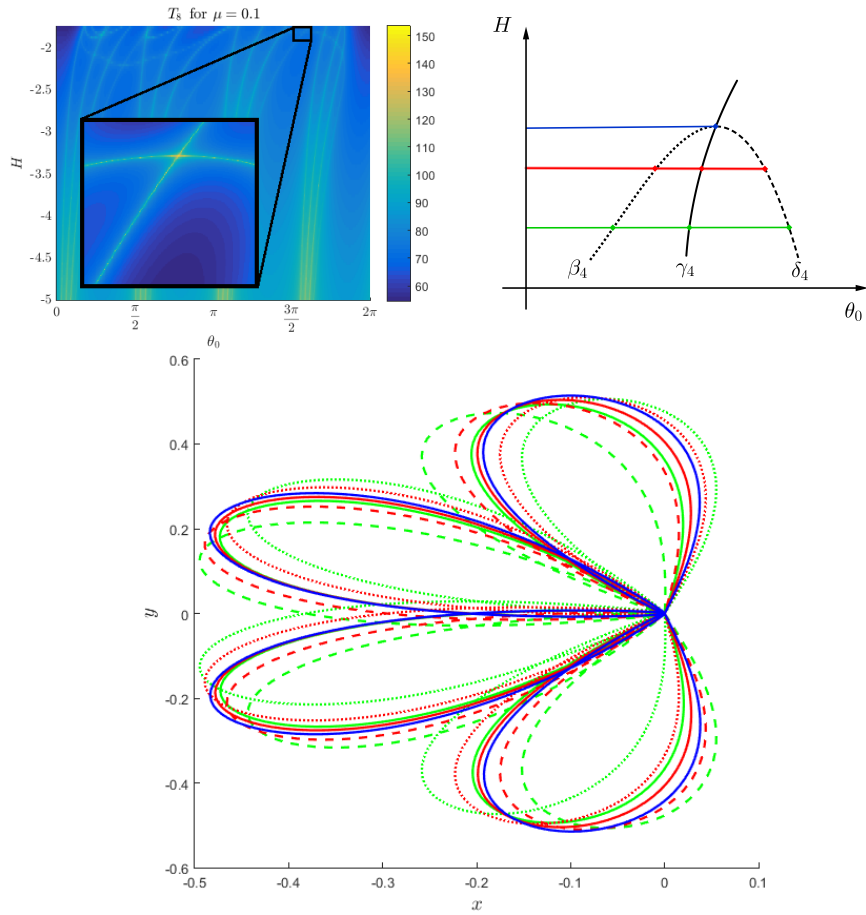


Figure 20: Collapse of families β_4 and δ_4 on to an orbit belonging to family γ_4 , for $\mu = 0.1$. *Top left.* An amplification of diagram (θ_0, H, T_8) . *Top right.* Qualitative plot in (θ_0, H) variables. We display the collapsing value of H in blue, and two less energetic values in red and green. *Bottom.* The orbits themselves. The one belonging to family γ_4 in blue, and the four bifurcated orbits for higher values of H in red and green.

described two strategies to detect and compute families of n -EC orbits. New bifurcating families of EC orbits, not known so far, have been obtained and

410 explained.

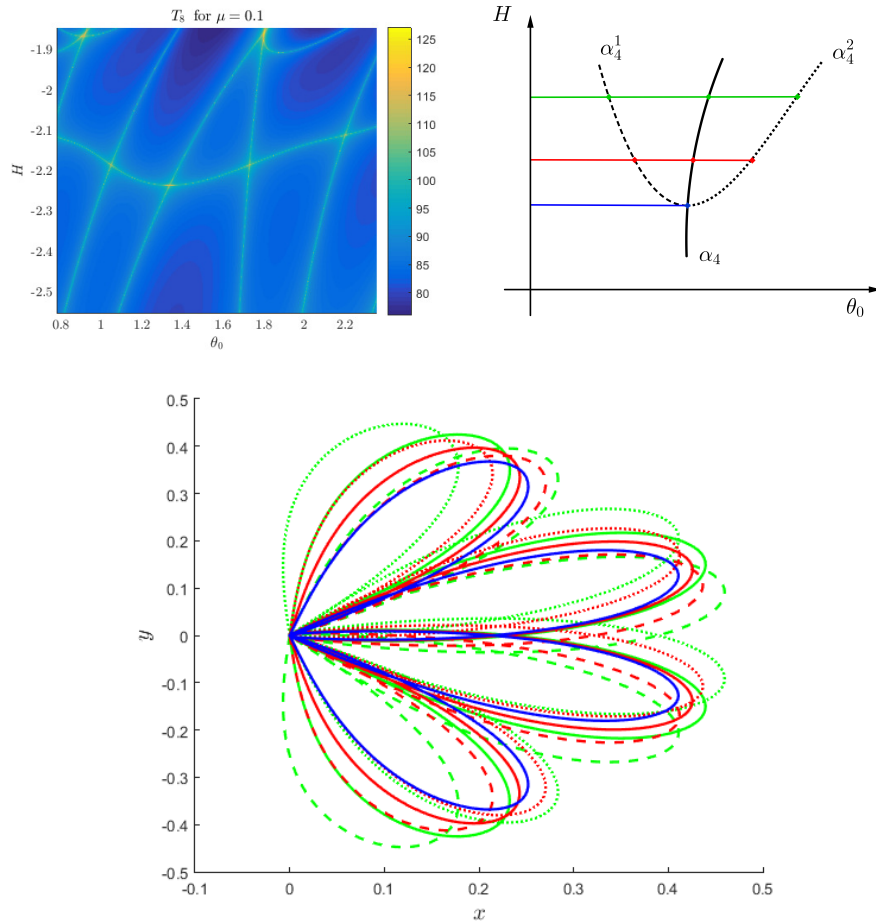


Figure 21: Bifurcation of 4-EC orbits for $\mu = 0.1$. *Top left.* An amplification of diagram (θ_0, H, T_8) . *Top right.* Qualitative plot of the bifurcating families in (θ_0, H) variables: dotted and discontinuous curves bifurcating from family α_4 (continuous curve). We display the limit value of H at the bifurcation in blue, and two more energetic values in red and green. *Bottom.* The orbits themselves. The one belonging to family α_4 in blue, and the four bifurcated orbits for higher values of H in red and green.

6. Acknowledgments

M. Ollé and O. Rodríguez have been supported by the Spanish MINECO/FEDER grant MTM2015-65715-P and the Catalan grant 2014SGR-00504. J. Soler has been supported by MINECO/FEDER grant number MTM2016-77278-P.

415 **References**

- [1] Barrabés, E., Mondelo, J. M., Ollé, M. Numerical continuation of families of homoclinic connections of periodic orbits in the RTBP. *Nonlinearity* 2009;22:2901–2918.
- [2] Bozis, G. Sets of collision periodic orbits in the Restricted problem. In: 420 *Periodic orbits, stability and resonances*, G.E.O. Giacaglia (eds). Holland: D. Reidel Pub. Co.; 1970, p. 176–191.
- [3] Chenciner, A and Llibre, J. A note on the existence of invariant punctured tori in the planar circular RTBP. *Ergod. Th. & Dynam. Sys.* 1988;8:63–72.
- [4] Hénon, M. Exploration numérique du problème restreint I. Masses égales, 425 *Orbites périodiques.* *Ann Astrophys* 1965;28:499–511.
- [5] Hénon, M. Numerical exploration of the Restricted Problem V. Hill’s case: Periodic orbits and Their Stability. *Astron Astrophys* 1969;1:223–238.
- [6] Lacombe, E. A. and Llibre, J. Transversal Ejection-Collision Orbits for the Restricted Problem and the Hill’s Problem with Applications. *J Differ* 430 *Equations* 1988;74:69–85.
- [7] Llibre, J. On the Restricted Three-Body Problem when the Mass Parameter is Small. *Celestial Mech Dynam Astronom* 1982;28:83–105.
- [8] Llibre, J, and Martinez-Alfaro, J. Ejection and collision orbits of the spatial RTBP. *Celestial Mech* 1985;35:113–128.
- [9] Llibre, J. and Pinyol, C. On the Elliptic Restricted Three-Body Problem. 435 *Celestial Mech Dynam Astronom* 1990;48:319–345.
- [10] McGehee, R. Triple Collision in the Collinear Three-Body Problem. *Invent Math* 1974;27:191–227.
- [11] McGehee, R. Singularities in Classical Celestial Mechanics. In: *Proceedings of the International Congress of Mathematicians Helsinki; 1978*, p. 827–834. 440

- [12] Pinyol, C. Ejection-collision orbits with the more massive primary in the planar elliptic restricted three-body problem. *Celestial Mech Dynam. Astronom* 1995;61:315–331.
- [13] Rodríguez, O. Òrbites d'ejecció-collisió en el problema restringit de tres
445 cossos. Master Thesis. Universitat Politècnica de Catalunya, 2016.
- [14] Szebehely, V. *Theory of orbits*. Academy Press, Inc., New York; 1967.